

*N63-12547
code-1*

NACA

RESEARCH MEMORANDUM

INVESTIGATION OF A 0.6 HUB-TIP RADIUS-RATIO TRANSONIC
TURBINE DESIGNED FOR SECONDARY-FLOW STUDY

II - DESIGN AND EXPERIMENTAL PERFORMANCE OF TURBINE WITH
LOW-VELOCITY-TURNING STATOR AND STANDARD ROTOR

By Harold E. Rohlik, William T. Wintucky, and Herbert W. Scibbe

Lewis Flight Propulsion Laboratory
Cleveland, Ohio

CLASSIFICATION CHANGED TO
UNCLASSIFIED - AUTHORITY:
NASA - EFFECTIVE DATE
SEPTEMBER 14, 1962

CLASSIFIED DOCUMENT

This material contains information affecting the National Defense of the United States within the meaning of the espionage laws, Title 18, U.S.C., Secs. 793 and 794, the transmission or revelation of which in any manner to an unauthorized person is prohibited by law.

**NATIONAL ADVISORY COMMITTEE
FOR AERONAUTICS**

WASHINGTON
July 18, 1957

NACA RM E57E09

2.60 ph
1.07 ref

XEROX \$
MICROFILM \$

UNCLASSIFIED

NACA RM E57E09

CONFIDENTIAL

NATIONAL ADVISORY COMMITTEE FOR AERONAUTICS

RESEARCH MEMORANDUM

INVESTIGATION OF A 0.6 HUB-TIP RADIUS-RATIO TRANSONIC
TURBINE DESIGNED FOR SECONDARY-FLOW STUDY

II - DESIGN AND EXPERIMENTAL PERFORMANCE OF TURBINE
WITH LOW-VELOCITY-TURNING STATOR AND STANDARD ROTOR

By Harold E. Rohlik, William T. Wintucky, and Herbert W. Scibbe

SUMMARY

A low-velocity-turning stator was designed to reduce secondary-flow loss cores by turning the flow at low velocities and accelerating it in passages of constant flow angle with reduced cross-channel pressure gradients. Performance of this stator was determined with static-pressure measurements and detailed surveys of total pressure and flow angle made with the turbine operating at design speed near design work. Turbine performance was measured to determine the effect of low-velocity turning in the stator on the over-all turbine performance.

The stator effectively eliminated loss cores in the suction-surface passage corners but developed very thick inner-wall boundary layers and blade wakes with an over-all total-pressure ratio of 0.964.

Stator losses affected rotor performance adversely and resulted in a maximum work at design speed of only 98.5 percent of the design value. Maximum turbine efficiency at design speed was 0.834, compared with 0.863 obtained with the same rotor and the standard stator.

Rotor exit surveys indicated a region of low efficiency and rotor underturning near the blade midspan, which resulted from rotor secondary flows and the large quantities of loss material in the stator.

INTRODUCTION

An investigation of the effects of stator and rotor secondary flows on over-all performance of a transonic turbine is being conducted at the NACA Lewis laboratory. These effects are being evaluated by studying the changes in over-all performance and internal flow conditions that result

UNCLASSIFIED

CONFIDENTIAL

from modification of secondary-flow patterns. Reference 1 presents the design and over-all performance of the standard turbine as well as a detailed picture of internal flow conditions at design-point operation of the turbine.

A turbine stator that turns air at low velocities and then accelerates it at constant flow angle to the design exit velocity has been designed, built, and tested so that low-velocity turning as a means of controlling turbine-stator secondary flows can be evaluated. This stator, which is a three-dimensional adaptation of the single-passage nozzle described in reference 2, was designed to keep loss accumulations at the suction-surface passage corners small by minimizing cross-channel flows on the passage end walls. Cross-channel pressure gradients exist only where turning of the air takes place. Since turning occurs only at low velocities, loss accumulations would be limited in magnitude. Acceleration is accomplished with a guided passage of design exit flow angle in which cross-channel pressure gradients are greatly reduced. This stator, however, is necessarily a compromise between reduced secondary-flow loss accumulation and the possibly greater losses incurred by the larger wetted area and end-wall curvature.

This report presents the design and experimental performance of the low-velocity-turning stator and the over-all performance of the turbine operated with this stator and with the standard turbine rotor. Results are compared with those obtained in a similar investigation with the same rotor and the stator described in part I of this series (ref. 1).

SYMBOLS

D	diffusion parameter
Δh	specific enthalpy drop, Btu/lb
l	mean camber length, ft
N	rotative speed, rpm
p	absolute gas pressure, lb/sq ft
r	radius, ft
U	blade velocity, ft/sec
V	absolute gas velocity, ft/sec
W	relative gas velocity, ft/sec

- w weight flow, lb/sec
- β relative gas-flow angle measured from axial direction, deg
- γ ratio of specific heats
- δ ratio of inlet-air total pressure to NACA standard sea-level pressure of 2116 lb/sq ft

ϵ function of $\gamma, \frac{\gamma_{sl}}{\gamma} \left[\frac{\left(\frac{\gamma + 1}{2} \right)^{\frac{\gamma}{\gamma - 1}}}{\left(\frac{\gamma_{sl} + 1}{2} \right)^{\frac{\gamma_{sl}}{\gamma_{sl} - 1}}} \right]$

- η total efficiency; ratio of turbine work based on torque, weight flow, and speed measurements to ideal work based on inlet total temperature, and inlet and outlet total pressure, both defined as sum of static pressure plus pressure corresponding to gas velocity calculated from flow area and continuity
- η_x rating efficiency; ratio of turbine work based on torque, weight flow, and speed measurements to ideal work based on inlet total temperature, and inlet and outlet total pressure, both defined as sum of static pressure plus pressure corresponding to calculated average axial component of velocity
- θ^* momentum-loss parameter
- θ_{cr} squared ratio of critical velocity at turbine inlet to critical velocity at NACA standard sea-level temperature, $V_{cr}/V_{cr,sl}$
- $\bar{\theta}$ effective rotor momentum thickness based on measured turbine performance

Subscripts:

- cr conditions at Mach number of 1.0
- h hub
- sl NACA standard sea-level conditions
- t tip
- tot sum of suction- and pressure-surface quantities

4

- u tangential direction
- x axial direction
- 0 station upstream of stator
- 1 station in stator-blade row at end of turning
- 2 station at outlet of stator just upstream of trailing edge
- 3 station at free-stream condition between stator and rotor
- 4 station at throat at rotor passage
- 5 station at outlet of rotor just upstream at trailing edge
- 6 station downstream of turbine

Superscript:

- ' absolute total state

STATOR DESIGN

The low-velocity-turning stator was designed for the same exit flow condition as the standard stator of reference 1. Figure 1 shows velocity diagrams for the turbine. The stator is a three-dimensional adaptation of nozzle 3 of reference 2, which was designed for an inlet Mach number of 0.1, turning through 60° to a Mach number of 0.2, and then accelerating to sonic velocity in a straight section with constant width and converging end walls. Experimental results obtained with this two-dimensional nozzle (ref. 2) showed that the maximum loss in total pressure in the secondary-flow loss accumulation was only 4 percent, compared with a maximum total-pressure loss of 20 percent for nozzle 1 (ref. 2), which was a comparable two-dimensional nozzle of conventional turbine stator area and velocity distribution. The nozzle designed for low-velocity turning, however, had an appreciably greater wetted flow area and consequently thicker wall boundary layers.

Turning Section

The first consideration in selecting the form of the low-velocity-turning stator was the prescribed exit geometry: (1) a cylindrical annulus with a 0.6 hub-tip radius ratio and (2) a particular radial variation in flow angle. These conditions precluded duplicating the form of the single

UNCLASSIFIED

passage of reference 2. Numerous modifications of the single-passage concept were considered and rejected in favor of a vaned stator of annular cross section at all axial locations. This stator has a greater annular area in the turning section than at the outlet.

A range of hub and tip radii was considered in selecting the dimensions of the large area turning section. Figure 2 shows the effect of variations in radius ratios on the level of velocity (in ratio form) at the hub at the completion of turning. Each curve of constant tip radius ratio has a minimum hub critical velocity ratio at a particular hub-tip radius ratio. At higher ratios the velocity increases because of the decrease in flow area, while at lower ratios the increase in flow area is offset by the greater radial span, which, from equilibrium considerations, causes a greater difference between hub and tip velocities.

The design point shown on figure 2 was selected because of three considerations. The first was the requirement of relatively low velocities during turning, which results in a low limit of possible maximum pressure loss in the secondary-flow loss accumulations, so that subsequent acceleration without turning will cause mixing of the accumulations and simple boundary-layer growth on the passage walls. The design point selected specifies critical velocity ratios of 0.49 and 0.29 at hub and tip, respectively. The dynamic head at any point in the flow represents the maximum possible total-pressure loss. The maximum possible losses corresponding to these velocity ratios are 13 percent of the free-stream total pressure at the inner wall and 5 percent at the outer wall, compared with maximum possible losses of 68 and 38 percent of the total pressure at the completion of turning in a conventional stator designed for the same exit flow condition.

The second consideration was tip diameter. A minimum consistent with the first requirement was desired, since this would minimize the necessary axial length and wetted area. The tip radius ratio selected provides velocities that are somewhat higher than those of the single passage reported in reference 2 but are still much lower than those of the stator exit; these velocities were considered satisfactory for evaluating the effect of low-velocity turning on turbine performance. Lower values of tip radius ratio were considered unsatisfactory because of the higher velocities.

The third consideration in selecting a design point on figure 2 was that of inner-wall geometry. The design point selected is considered most satisfactory in this respect, because it requires no inner-wall curvature and provides the minimum velocity for the tip diameter selected. Inner-wall curvature is undesirable, because the curvature at the point where the inner-wall radius approaches the stator exit radius would be of the same sign as curvature about the axis of rotation, which would cause a local acceleration in a high-velocity region and possible flow separation. Outer-wall curvature is not objectionable because of the lower velocities encountered.

UNCLASSIFIED

The fabrication method selected specified 0.050-inch sheet-metal blades fastened by inner- and outer-wall spacers contoured to the passage shape. The need for sealing the clearances made easy accessibility of all parts of the passage desirable. This led to the selection of 12 blades and consequently large passage areas.

The blade passages in the turning part of the stator were laid out at hub, mean, and tip radii, and velocities were calculated by the method of reference 1. The surface and midchannel velocities for this part of the stator are shown in figure 3.

Constant-Angle Section

A single check of velocity in the constant-angle part of the stator (downstream of station 1) was made to determine whether the outer-wall configuration resulted in velocity levels substantially greater than the outer-wall exit velocity. A streamline geometry in a radial-axial plane of axisymmetric flow was assumed in the calculation to obtain velocities along a line normal to streamlines in this plane. The normal line selected intersected the outer wall near the exit, where outer-wall curvature is high and the likelihood of a velocity peak is greatest. The calculation satisfied equilibrium and continuity along this normal line, using equations (3) and (5) of reference 3. The solution was approximate because axial symmetry was assumed, but it was considered adequate as a check on midchannel velocity level. The critical velocity ratios calculated for this normal line were 0.92 at the inner wall and 0.84 at the outer wall. The outer-wall geometry therefore was considered satisfactory, and no further calculations were made. Figure 4 shows a cross section of the stator, and figure 5 shows an axial view of one blade. The circumferential span at the hub (139°) is considerably greater than that at the tip (69°); this results from the smaller helix angles and the smaller radius.

APPARATUS, INSTRUMENTATION, AND PROCEDURE

The apparatus, instrumentation, and method of calculating the performance parameters were the same as those used in reference 1 with the exception of the turbine stator; the stator used is shown in figure 6. In addition, static pressures were measured along the inner- and outer-wall midchannel of one stator passage by means of eleven outer-wall static taps located approximately 1.0, 2.0, 3.0, 4.0, 5.0, 6.0, 6.5, 7.0, 7.5, 8.0, and 9.0 inches, and eleven inner-wall static taps located approximately 2.5, 3.25, 4.0, 4.75, 5.5, 6.0, 6.5, 7.0, 7.5, 8.0, and 9.0 inches axially downstream of the leading edge of the stator blades.

The methods of operating the turbine, obtaining over-all performance, and annular surveying were the same as those used in reference 1. Surveys at stator and rotor exit were made with the rotor operating at design speed and near design work.

RESULTS AND DISCUSSION

Stator Performance

Performance of the low-velocity-turning stator was determined with stator exit surveys of total pressure and flow angle and with wall static-pressure measurements throughout the stator, with the turbine operating at design speed and near design work.

Figure 7 shows the inner- and outer-wall distributions of the ratio of midchannel static pressure to inlet total pressure through the low-velocity-turning stator. Smooth acceleration is indicated along the entire inner wall with a terminal value of pressure ratio somewhat lower than the design value. The low exit values indicate that the stator was slightly overexpanded at this turbine operating point. Flow along the outer wall showed the effects of wall curvature, with a small velocity peak indicated near the stator exit where the wall curvature is high and opposite in sign from curvature about the axis of rotation. The experimental value of pressure ratio at this point is 0.657, compared with the theoretical value of 0.626. This degree of agreement is somewhat fortuitous in view of the approximate nature of the theoretical calculation and the location of the static taps, but it confirms the location and approximate velocity level determined in the design procedure.

The results of the stator exit surveys of total pressure were used to plot the contours of total-pressure ratio shown in figure 8(a). These contours show thin outer-wall boundary layers but very thick inner-wall boundary layers. The blade wakes are comparable in magnitude of loss with the standard stator-blade wakes described in reference 1, but they cover a greater area. The inner-wall boundary layer shows thickened regions between blade wakes, which may be a result of either the loss cores occurring upstream or the radially inward flow of boundary layers on both suction and pressure sides of the passage. No loss cores are apparent, however, at the stator exit. The most prominent part of this loss pattern, the extremely thick inner-wall boundary layer, apparently is the result of the large wetted area in the stator that contributed to boundary-layer development and the radial pressure gradient that caused blade boundary layers to flow toward the inner wall. For comparison, figure 8(b) shows loss contours from reference 1 for the standard stator.

The survey data used in preparing the loss contours of figure 8 were also used to compute a radial distribution of the momentum-loss parameter for each stator (fig. 9). The momentum loss for the low-velocity-turning stator is much greater in the inner-wall boundary layer than the loss for the standard stator and is slightly greater in the rest of the blade passage. The calculated over-all total-pressure ratio for the low-velocity-turning stator was 0.964, compared with 0.975 for the standard stator. This difference would account for a drop in turbine efficiency of 0.011 at design work if rotor performance remained constant.

The stator-exit static pressures and surveys of total pressure and flow angle were used to compute a radial distribution of moment of momentum in order to check the performance of the stator in terms of work potential for the rotor. The distribution indicated by these measurements (fig. 10) shows greater than design moment of momentum throughout the free stream. The mass-averaged value of this parameter at design turbine speed and maximum work was 2.6 percent higher than the design value. Angle surveys, however, showed underturning of 5.2° near the blade midspan.

The radial distribution of relative inlet flow angle, calculated from known pressures, total temperature, flow angle, and wheel speed, is shown in figure 11 along with the design distribution. The maximum incidence angle is 4° .

Over-all Turbine Performance

Figure 12 shows turbine equivalent specific work plotted against weight-flow - speed parameter with contours of percent equivalent design speed, pressure ratio, and efficiency. Maximum work at design speed was 21.37 Btu per pound, or 98.5 percent of design work. This fact, in combination with the measured moment of momentum at the stator exit, indicates that rotor-blade performance was adversely affected by the stator loss distribution to the extent that considerably less than design turning was accomplished.

Total efficiency (fig. 12(a)) at design speed and near limiting work was 0.834. The combination of the standard stator and the same rotor operated with a total efficiency of 0.863 at this condition. The difference in efficiency is due partly to the greater losses incurred in the low-velocity-turning stator and partly to the poorer rotor-blade performance. Maximum total efficiency, 0.856, occurred at 120-percent design speed and near limiting loading.

Maximum rating efficiency at design speed (fig. 12(b)) was 0.832, indicating an exit-whirl loss of less than 0.01 in efficiency.

Rotor Exit Surveys

Annular surveys of total pressure and total temperature were used with turbine inlet conditions to obtain variations in local total efficiency at the rotor exit. Contours of efficiency at this station are shown in figure 13. The total-pressure surveys, as well as the efficiency contours, indicate that both wall boundary layers were quite thin in contrast to conditions at the stator exit, where the inner-wall boundary layer was very thick. The stator-blade wakes effected a loss in turbine efficiency that is apparent locally at the rotor exit. The heavy dashed line passes through regions of lowest efficiency at each radius, indicating the location of a stator-blade wake after passing through the rotor. This blade wake appears to be superimposed on a pattern of circumferential bands of efficiency that indicate high levels of efficiency near the end walls and a relatively wide band of lower efficiency at the blade midspan. This effect is shown more clearly in figure 14, which is a radial plot of circumferentially averaged local efficiencies for the turbine of this report as well as for the turbine of reference 1. The patterns are almost identical in shape but occur at different levels of efficiency. This pattern is believed to be a result of rotor secondary flows, as discussed in reference 1.

The radial pressure gradient at the stator exit results from the high level of whirl that drives low-velocity material toward the hub and results in a force that is greater than centrifugal forces acting on the rotor-blade boundary layers in the early part of the passage. Consequently, accumulation of low-velocity material at the rotor hub continues until the rotor passages turn the air sufficiently to bring the two radial forces into balance. Beyond this point, the centrifugal forces predominate, and low-velocity material in the rotor-blade wakes and boundary layers will move radially outward. The net result appears to be an accumulation of loss material near the blade midspan at the rotor exit.

Radial surveys of flow angle at the rotor exit show that the hub and tip portions of the rotor blades turn the air much more efficiently than the middle part of blades. The flow-angle variation from hub to tip was 15.4° , compared with the design variation of 2.7° . A calculated relative flow angle, determined with measured flow angle, velocity, and wheel speed, indicated underturning of 10° at the blade midspan. This underturning apparently was caused by the presence of loss material in the blade boundary layers, which adversely affected blade-element performance.

A single value of rotor effective momentum thickness, calculated as in reference 1 for turbine operation at design speed near design work, is shown in figure 15. This value is an index of the aerodynamic performance of the rotor and is appreciably higher (about 18 percent) than the value obtained with the same rotor and with the standard stator, indicating that the effect of the thickened stator inner-wall boundary layer and stator-blade wakes on rotor performance was to induce greater rotor losses.

SUMMARY OF RESULTS

The design of a low-velocity-turning turbine stator and the experimental performance of the turbine and its components have been described herein. Results may be summarized as follows:

1. Surveys of total pressure at the stator exit indicate effective elimination of secondary loss cores. This was accompanied however by the development of very thick inner-wall boundary layers and blade wakes, with a net loss of 0.011 in total pressure when compared with a conventional stator designed for the same application.

2. Maximum turbine work obtainable at design speed was only 98.5 percent of design work. This limit resulted from poor rotor performance induced by high localized losses at the stator exit, even though the stator set up more than design moment of momentum. Turbine efficiency at design speed near limiting loading was 0.834, compared with 0.863 for the combination of the same rotor and the standard stator. This drop in efficiency is the result of greater losses in the stator as well as poorer rotor performance.

3. Contours of local turbine efficiency from rotor exit surveys show the stator-blade wake loss pattern superimposed on circumferential bands of efficiency developed in the rotor. The predominant part of this efficiency pattern, the presence of a low-efficiency region near the midspan with much higher efficiencies near both end walls, is believed to be the result of rotor secondary flows which redistribute losses developed in the stator as well as the rotor. The region near the blade midspan also included poor rotor performance with regard to turning, with about 10° less turning than in the region near the end walls.

Lewis Flight Propulsion Laboratory
National Advisory Committee for Aeronautics
Cleveland, Ohio, May 13, 1957

REFERENCES

1. Rohlik, Harold E., Wintucky, William T., and Scibbe, Herbert W.: Investigation of a 0.6 Hub-Tip Radius-Ratio Transonic Turbine Designed for Secondary-Flow Study. I - Design and Experimental Performance of Standard Turbine. NACA RM E56J16, 1957.
2. Stewart, Warner L., and Wong, Robert Y.: Low-Velocity Turning as a Means of Minimizing Boundary-Layer Accumulations Resulting from Secondary Flows Within Turbine Stators. NACA RM E54B16, 1954.

UNCLASSIFIED

NACA RM E57E09

CONFIDENTIAL

11

3. Stewart, Warner L.: Analytical Investigation of Flow Through a High-Speed Mixed-Flow Turbine. NACA RM E51H06, 1951.
4. Stewart, Warner L., Whitney, Warren J., and Miser, James W.: Use of Effective Momentum Thickness in Describing Turbine Rotor-Blade Losses. NACA RM E56B29, 1956.

UNCLASSIFIED

CONFIDENTIAL

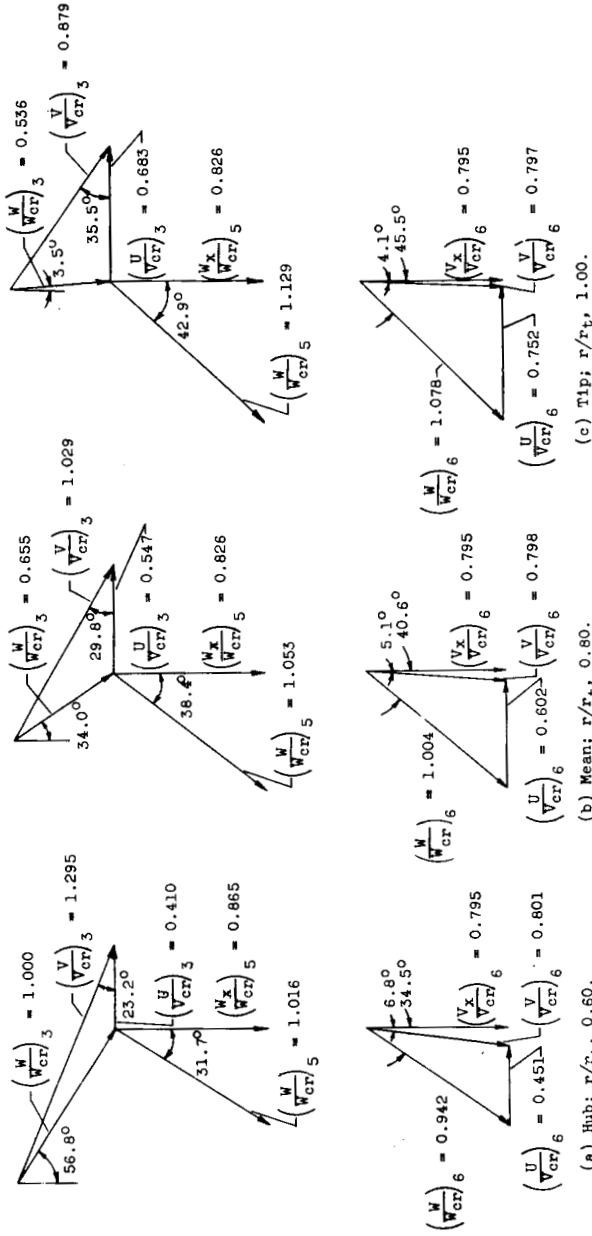
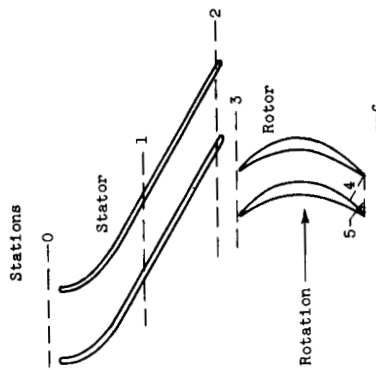


Figure 1. - Design velocity diagrams of transonic secondary-flow turbine.



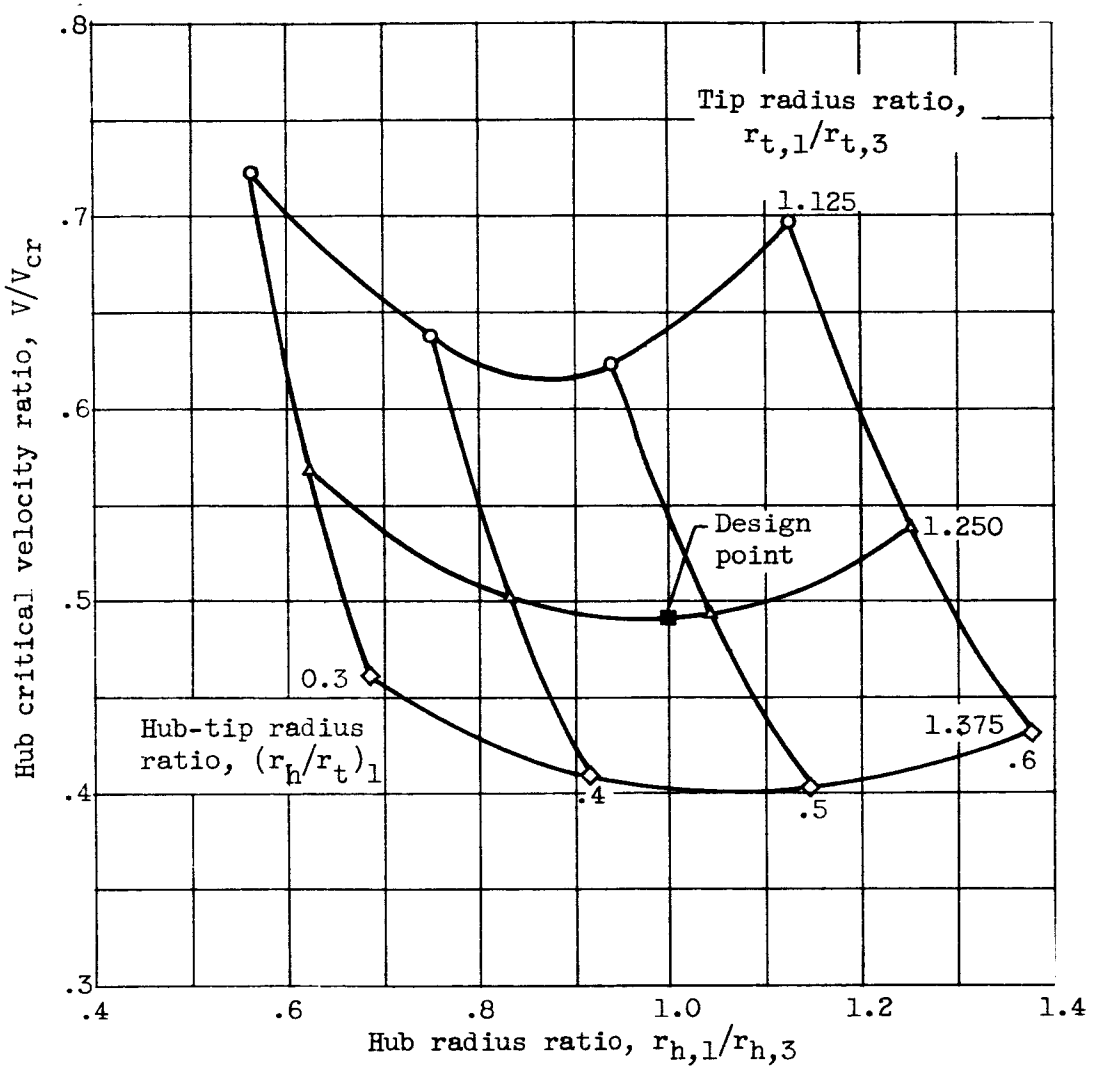


Figure 2. - Variation of hub critical velocity ratio at end of turning section over range of hub and tip radii.

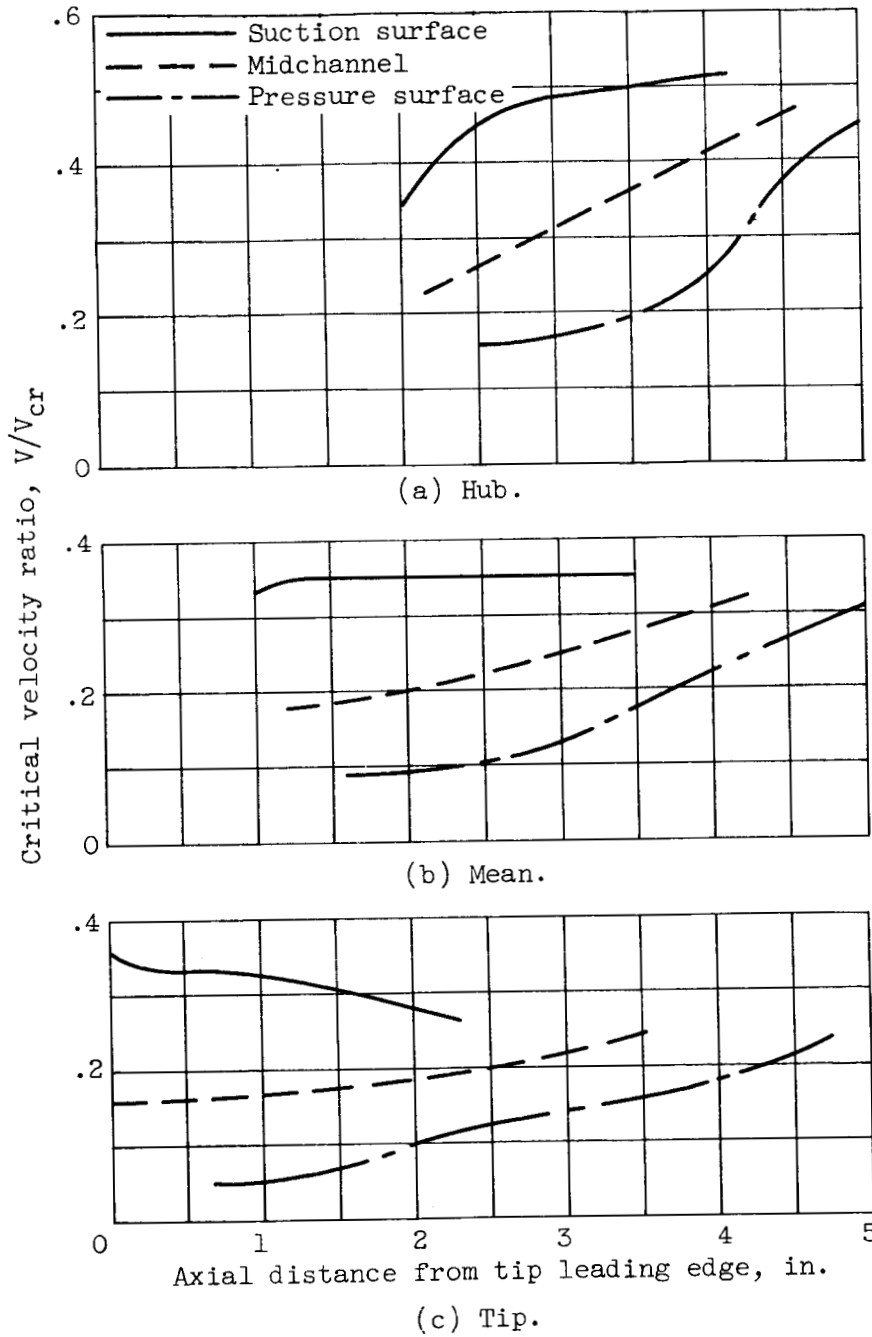
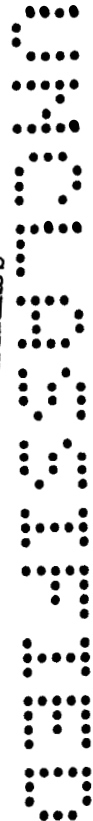


Figure 3. - Channel velocities in turning section of low-velocity-turning stator.



CONFIDENTIAL

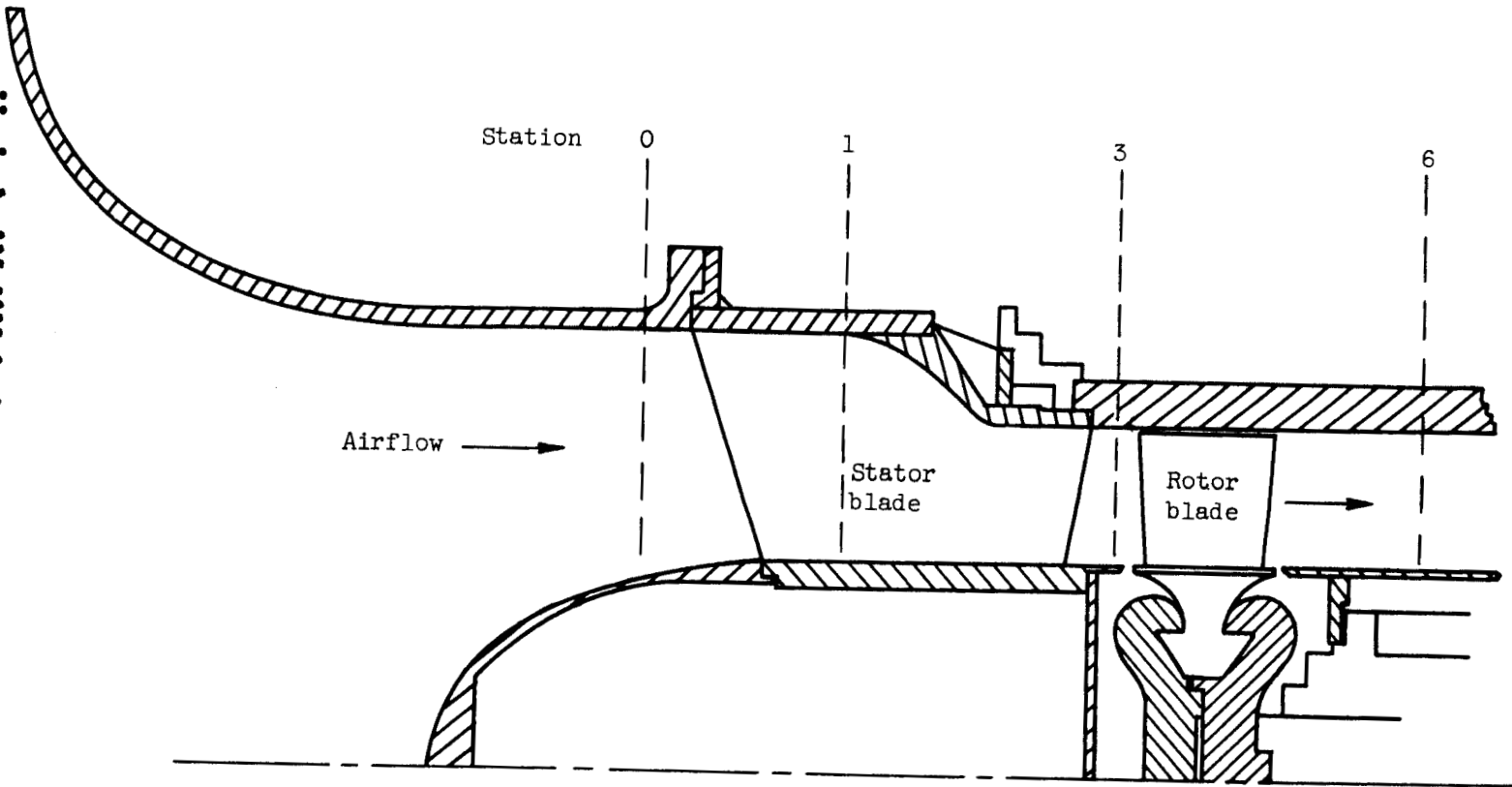


Figure 4. - Diagrammatic sketch of turbine test section with low-velocity-turning stator.

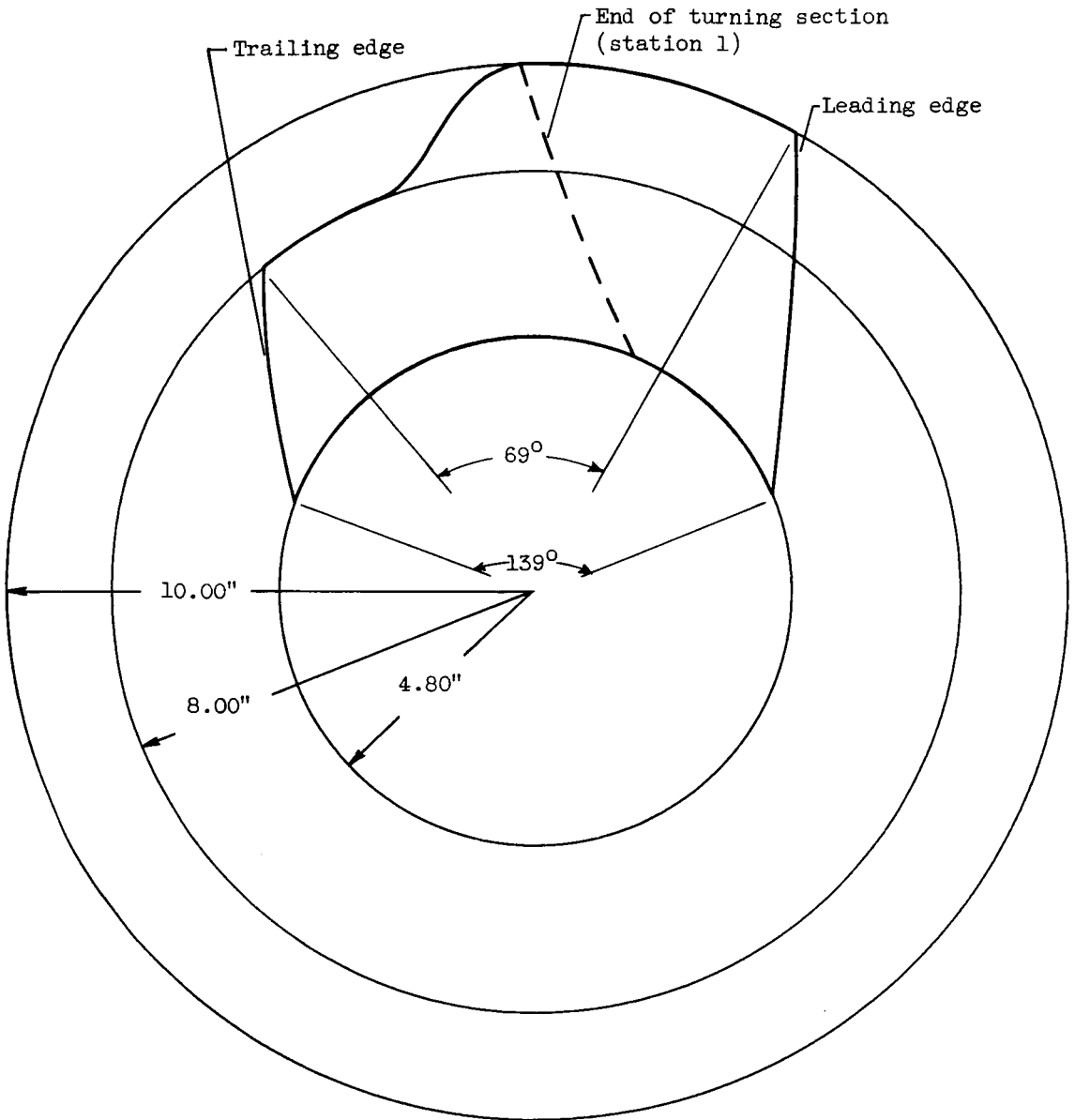
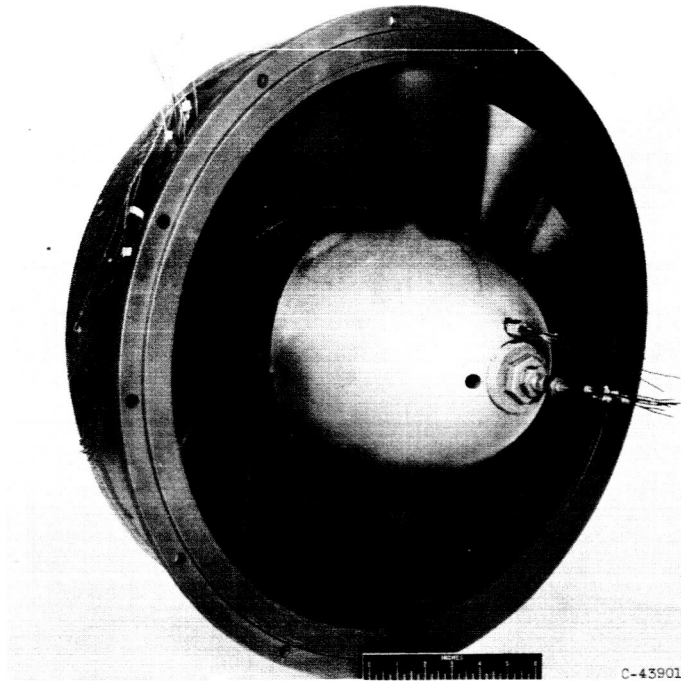
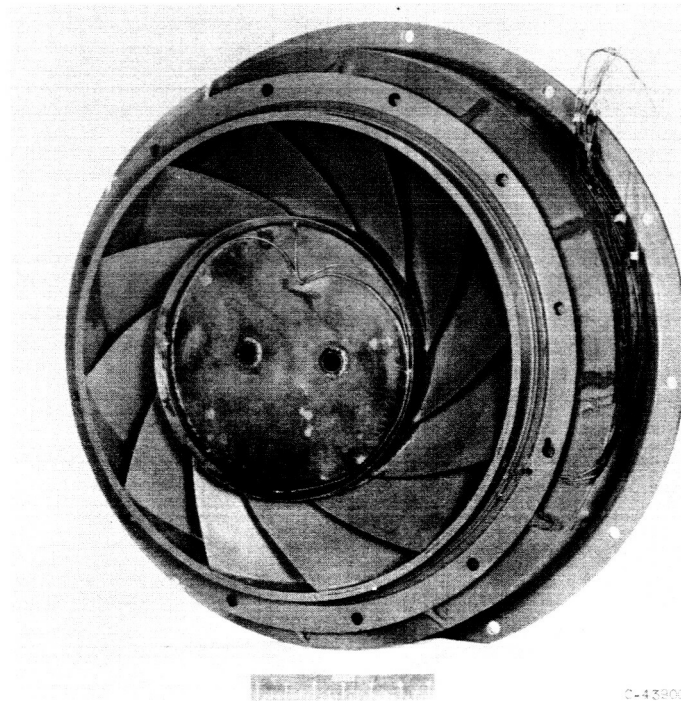


Figure 5. - Axial view of low-velocity-turning stator blade.



(a) Upstream view.



(b) Downstream view.

Figure 6. - Low-velocity-turning stator.

CONFIDENTIAL

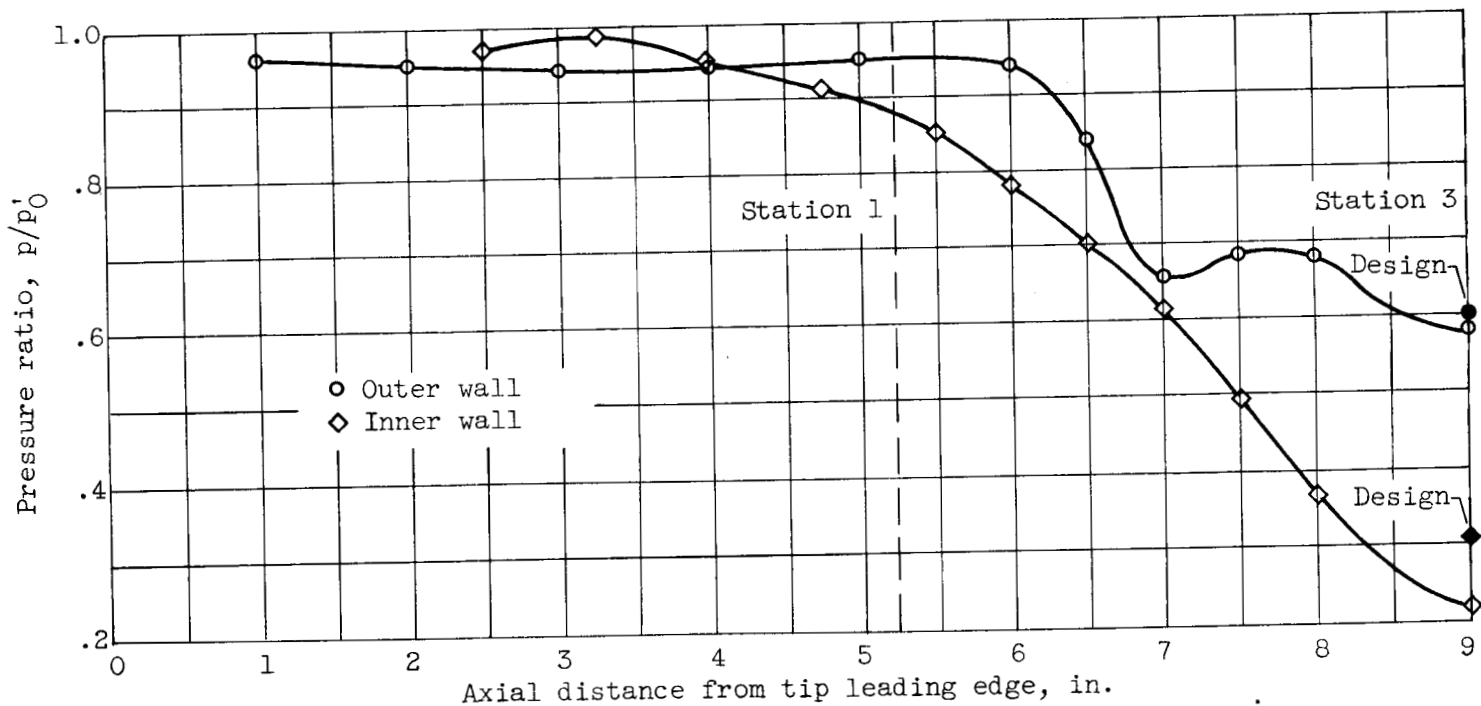
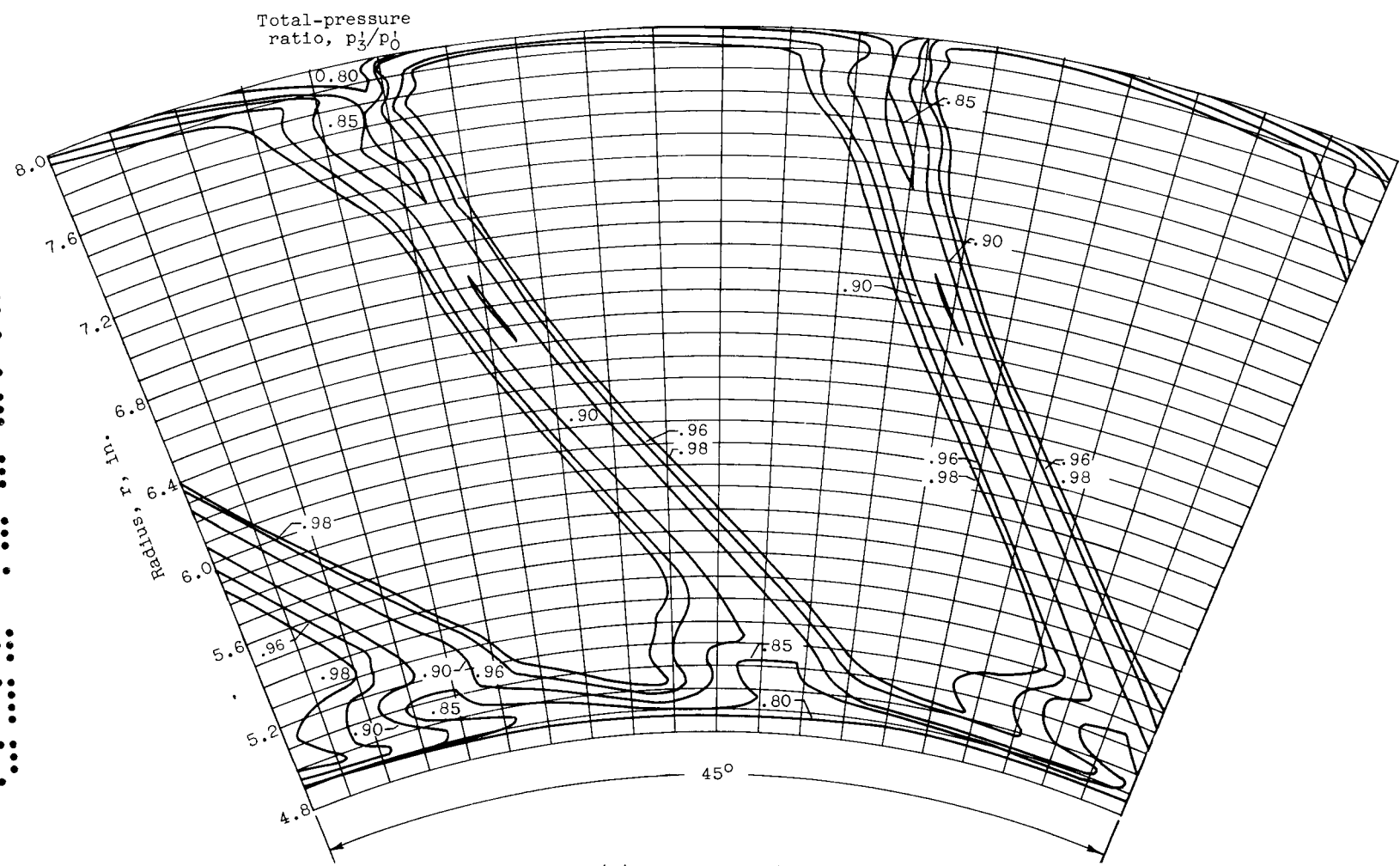


Figure 7. - Axial variation of ratio of midchannel wall static pressure to inlet total pressure through low-velocity-turning stator.

CONFIDENTIAL

CONFIDENTIAL

CONFIDENTIAL



(b) Standard stator.

Figure 8. - Concluded. Contours of total-pressure ratio at exit measuring station.

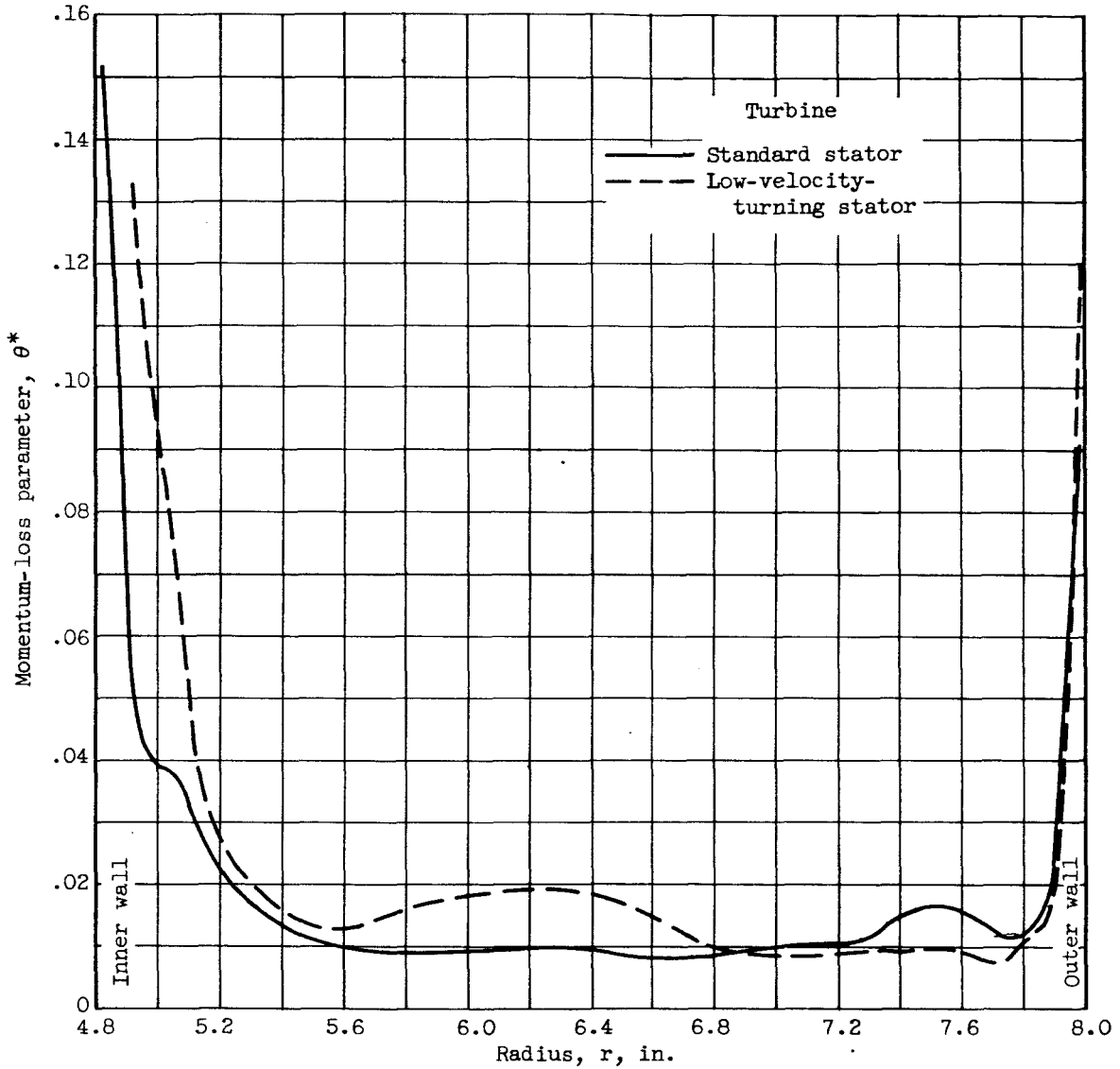


Figure 9. - Radial distribution of momentum-loss parameter at stator-exit survey station.

CONFIDENTIAL

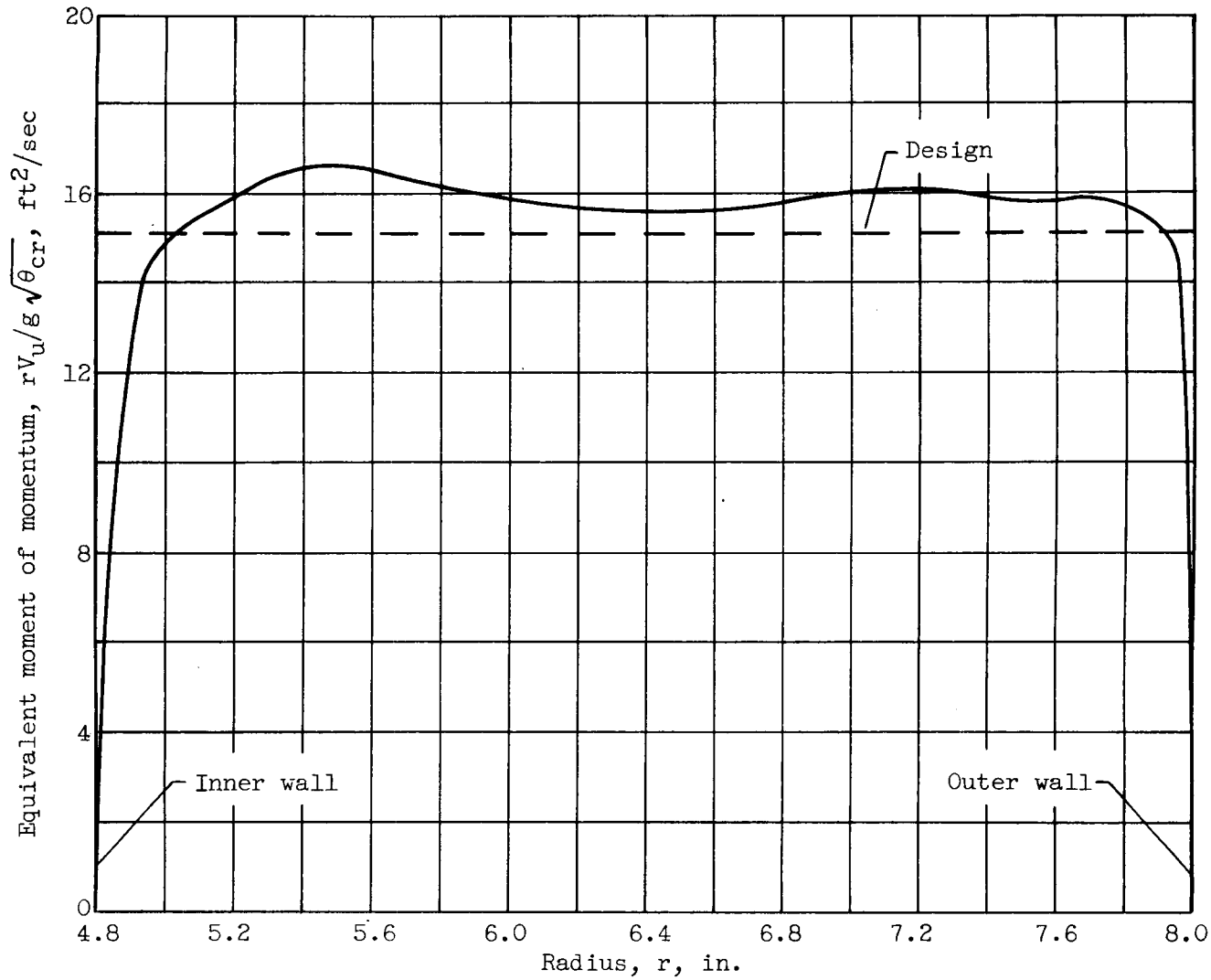


Figure 10. - Radial distribution of equivalent moment of momentum at exit of low-velocity-turning stator.

CONFIDENTIAL

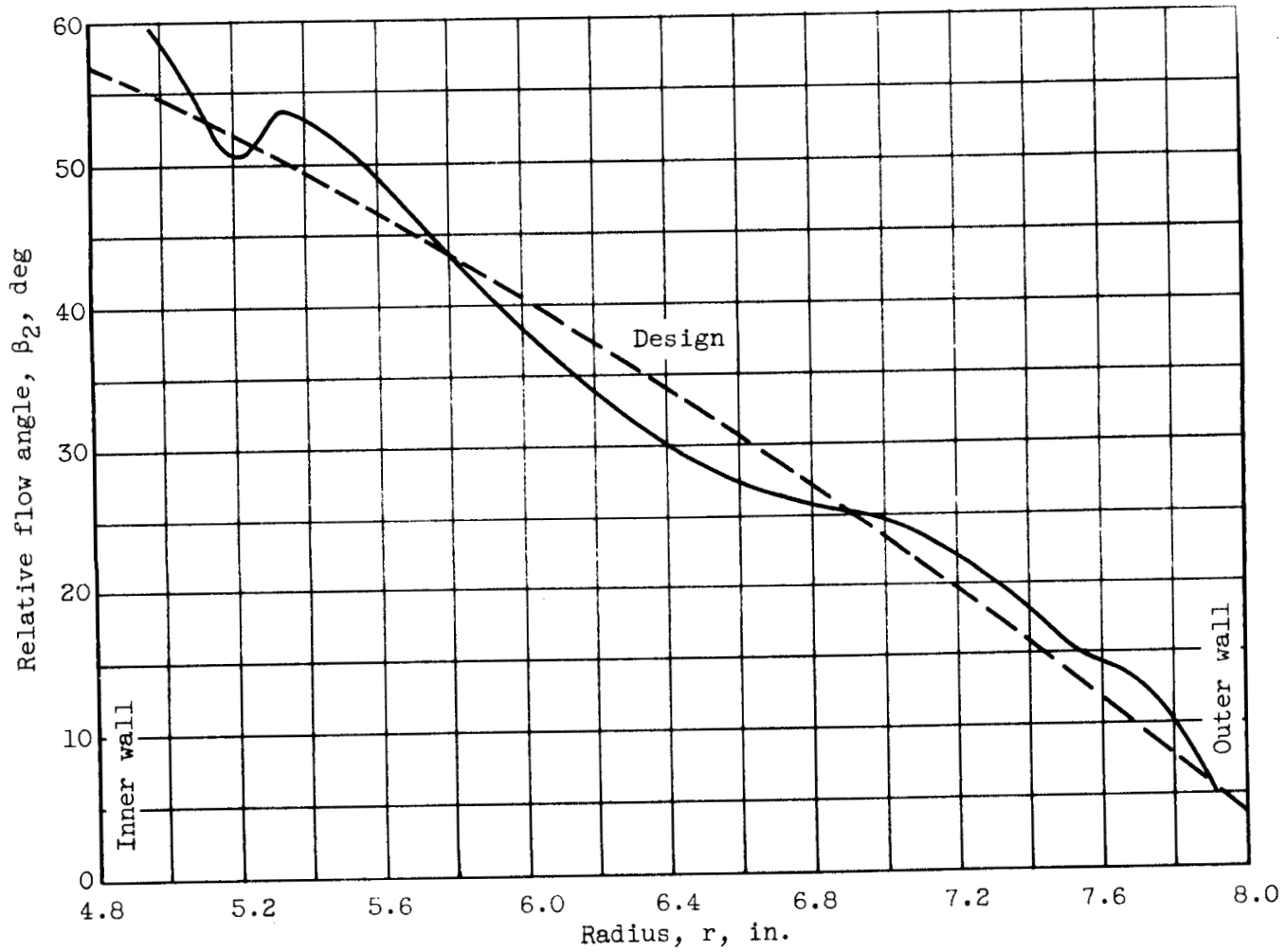
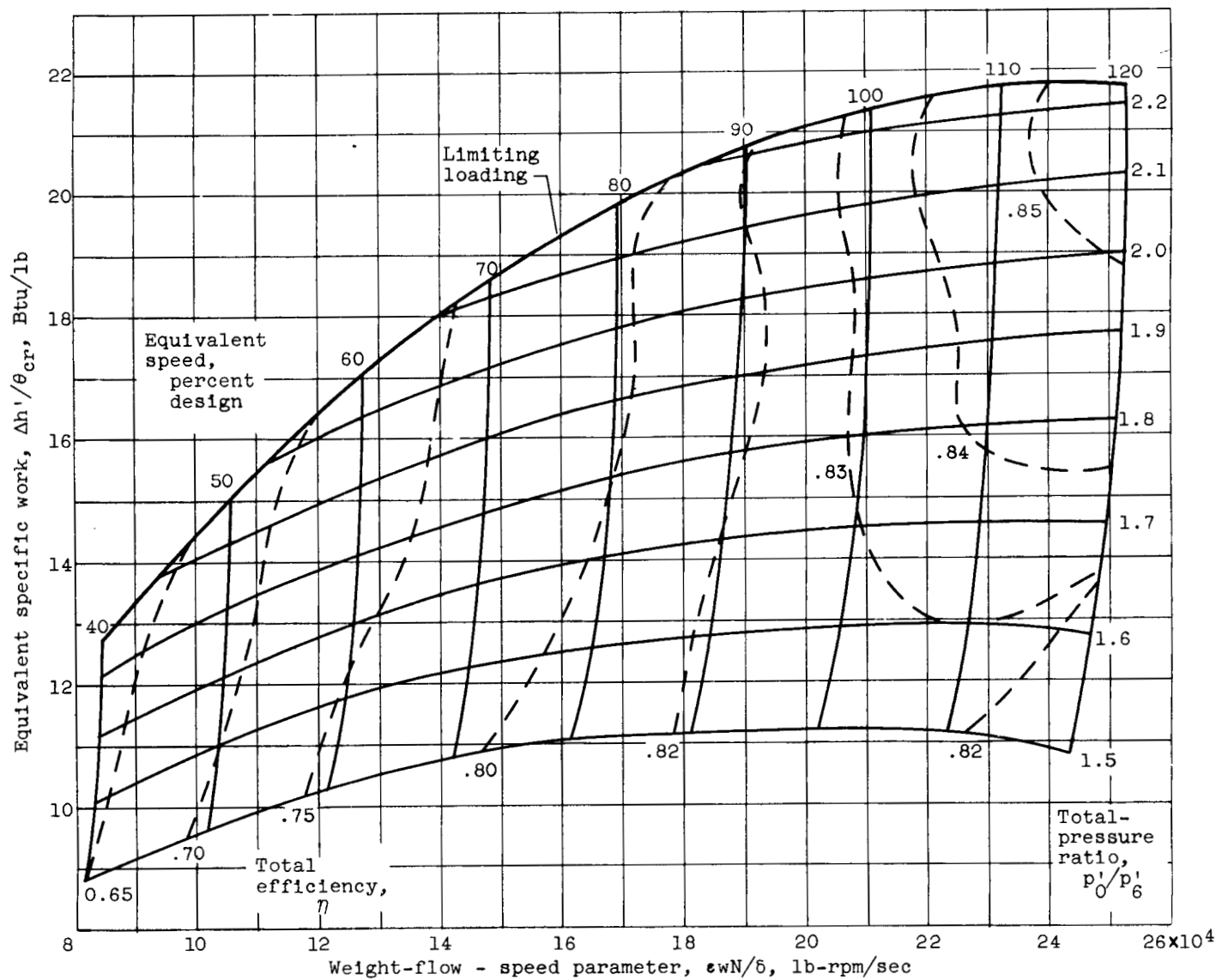


Figure 11. - Radial variation of relative flow angle at rotor exit.

CONFIDENTIAL

CONFIDENTIAL

CONFIDENTIAL



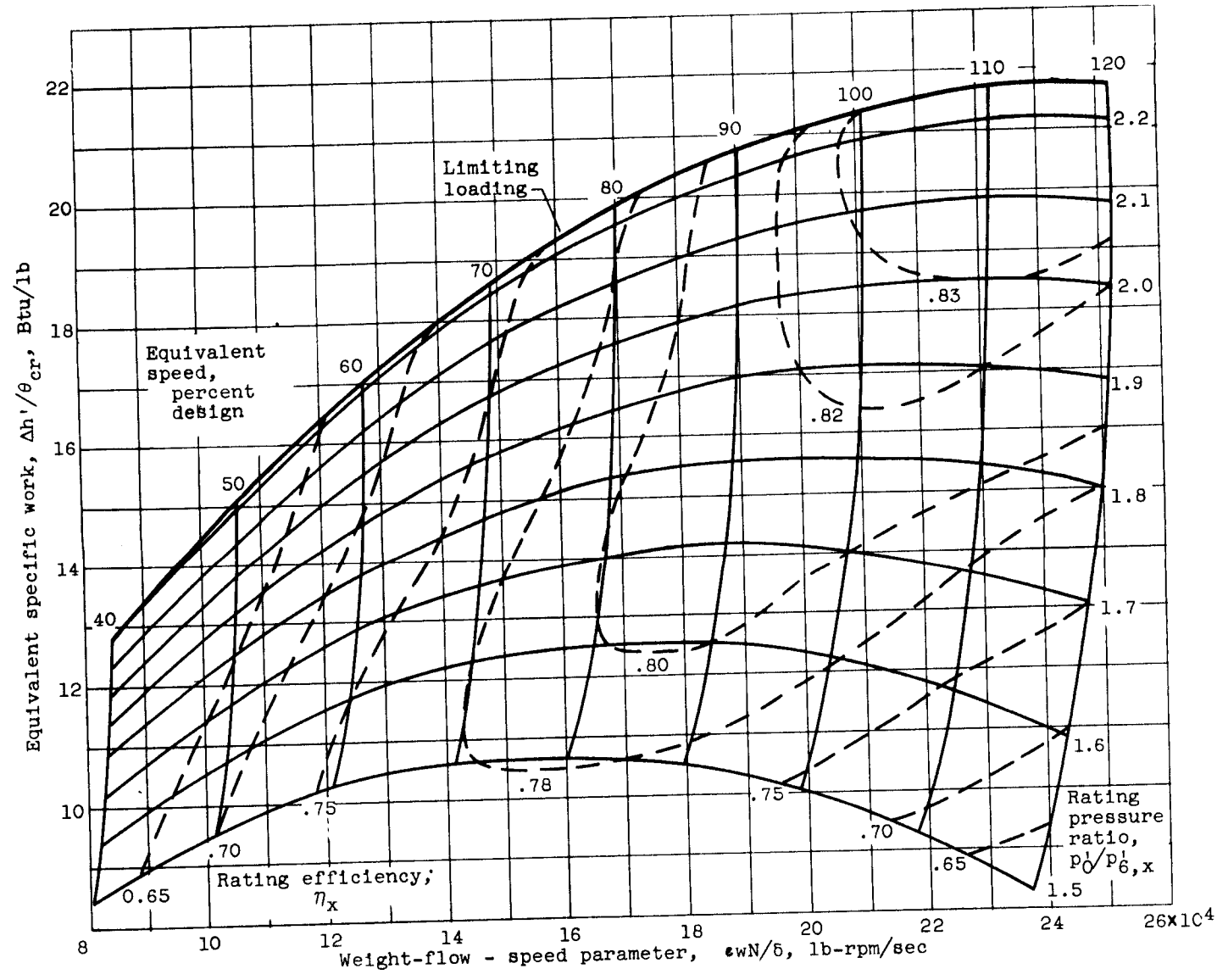
(a) Based on total-pressure ratio.

Figure 12. - Over-all turbine performance.

CONFIDENTIAL
NACA RM E57E09

CONFIDENTIAL

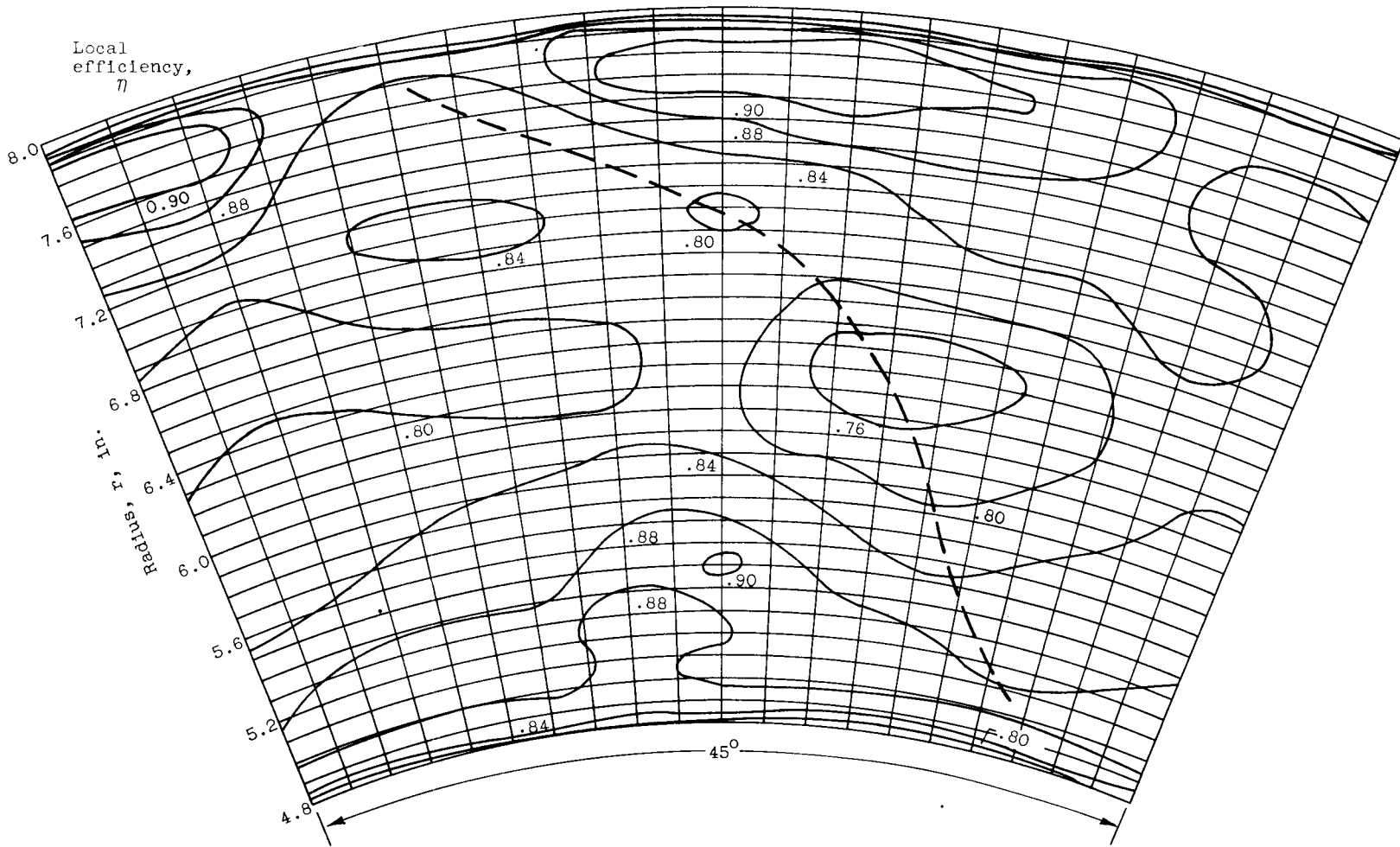
CONFIDENTIAL



(b) Based on rating pressure ratio.

Figure 12. - Concluded. Over-all turbine performance.

CONFIDENTIAL
IACA RM E57E09



Local efficiency, η

Radius, r , in.

45°

Figure 13. - Contours of local efficiency at rotor exit from surveys made at design speed near design work.

CONFIDENTIAL

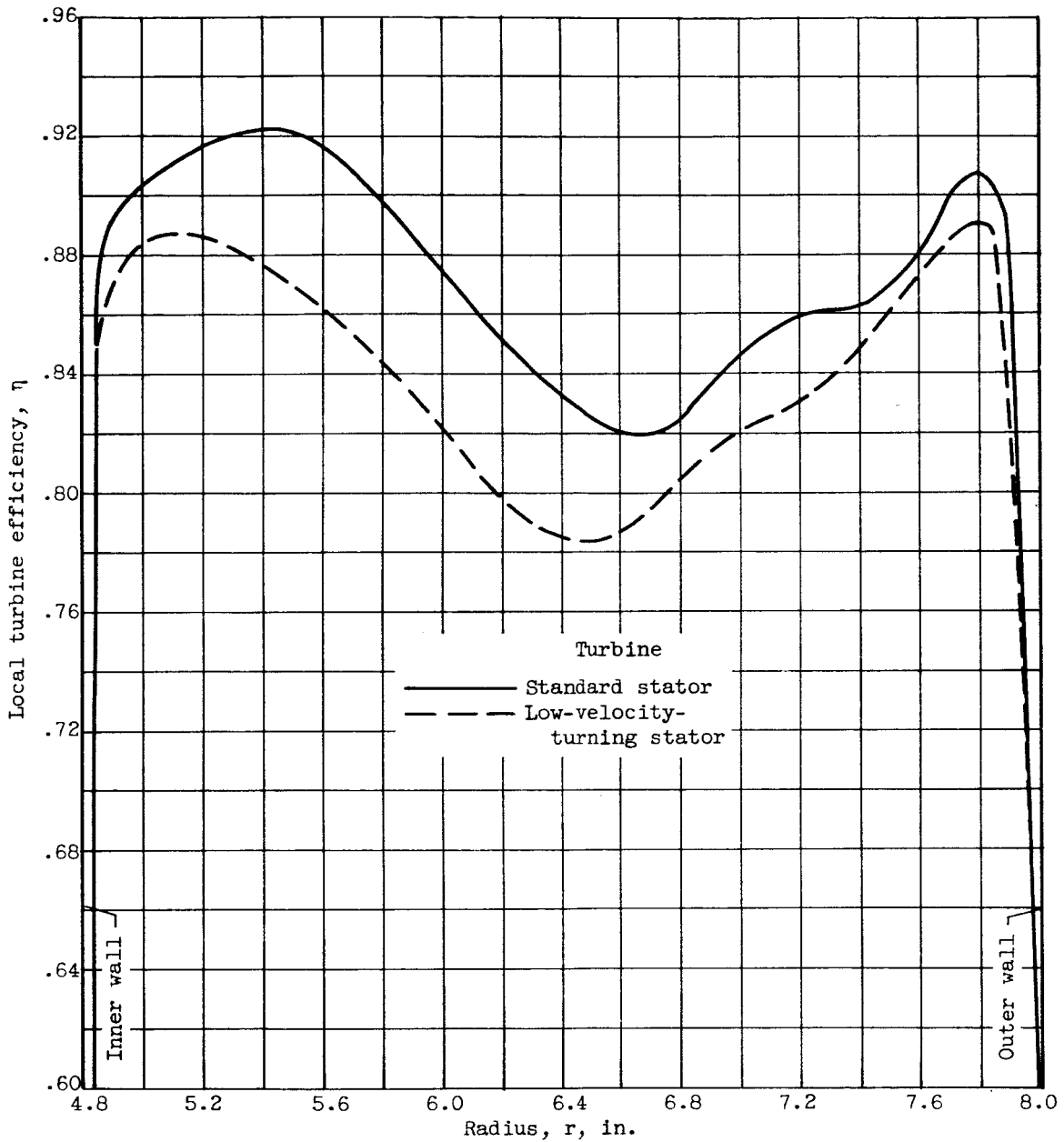


Figure 14. - Radial distribution of circumferentially averaged local efficiency from rotor exit surveys.

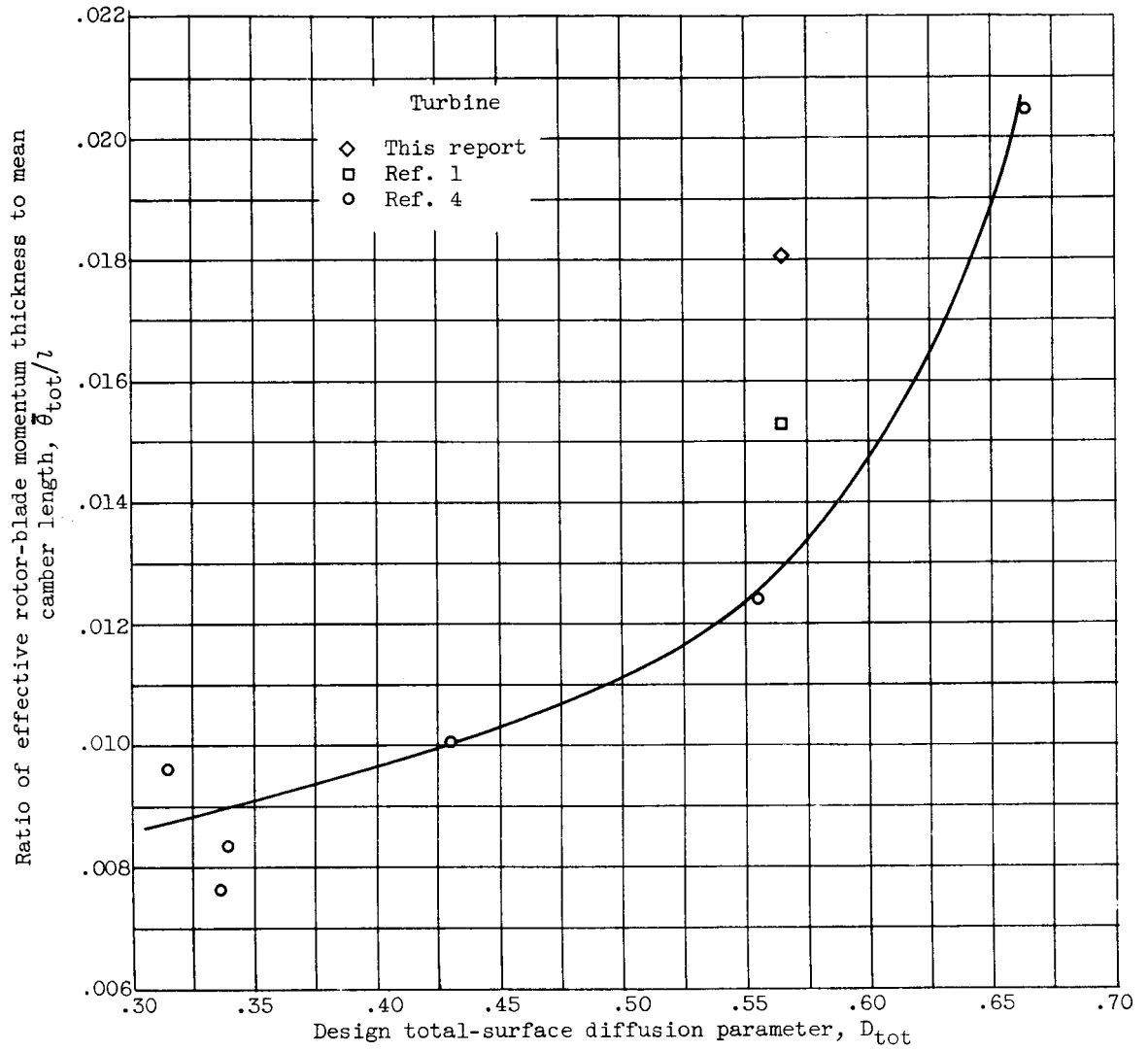


Figure 15. - Variation in ratio of effective rotor-blade momentum thickness to mean camber length with design total-surface diffusion parameter.

CONFIDENTIAL

CONFIDENTIAL